Detection of Protein Orientation on the Silica Microsphere Surface Using Transverse Electric/Transverse Magnetic Whispering Gallery Modes

Mayumi Noto, David Keng, Iwao Teraoka, and Stephen Arnold
Microparticle Photophysics Laboratory, Polytechnic University, Brooklyn, New York 11201

ABSTRACT The state of adsorbed protein molecules can be examined by comparing the shifts in a narrow line resonance wavelength of transverse electric (TE) and transverse magnetic (TM) whispering gallery modes (WGM) when the molecules adsorb onto a transparent microsphere that houses WGM. In adsorption of bovine serum albumin (BSA) onto an aminopropyl-modified silica microsphere, the TM/TE shift ratio indicated highly anisotropic polarizability of BSA in the direction normal to the surface, most likely ascribed to anchoring the heart-shaped protein molecule by one of its tips. The polarization-dependent resonance shift was confirmed when the surrounding refractive index was uniformly changed by adding salt, which would simulate adsorption of large objects.

INTRODUCTION

The quantity and quality of protein adsorbed on a surface is of a great concern (1–4). The amount of the surface-bound protein can be evaluated by various methods (2–11). However, methods to find the state of the adsorbed molecules are not well established, except that submolecular information can be obtained using spectroscopic methods (8–10). There are controversies about the state and orientation of adsorbed molecules, even for often studied proteins such as serum albumin (2,4,11). Their conformation may depend on the surface—whether it is hydrophobic or ionic (positively or negatively charged)—and on the pH of the immersing aqueous phase. This article proposes using resonance shifts of photonic whispering gallery modes (WGM) as a method to determine the state of adsorbed protein.

A transparent microsphere can accommodate WGM in the vicinity of the sphere surface. The light propagates near the curved surface by total internal reflection. Resonance is achieved when the light path closes upon itself in phase after one cycle. If the diameter of the sphere is sufficiently large compared with the wavelength, the resonance can have a narrow width. The Q value of a silica microsphere in water at a 1.3-μm wavelength can be as large as 2×10^6 (12). A much greater Q value, exceeding 10^8, is reported for a toroidal resonator at 680 nm (13).

In each reflection along the circular path of WGM, the light seeps into the surroundings as an evanescent wave. The wavelength of the sharp resonance is sensitive to small changes in dielectric property in the immediate neighborhood of the transparent microsphere (14). The changes include adsorption of molecules onto the microsphere and a change of refractive index (RI) in the surrounding medium. The shift of the wavelength upon adsorption of biomolecules onto the microsphere has been heralded as the most sensitive detector ever made possible without the necessity for fluorescent labeling (12,15–18). Detection of a single protein molecule is considered within reach (15). Recent prediction (19) and demonstration (20) of enhanced sensitivity by a high RI coating has paved the way for the difficult detection. The sensor's capability is not limited to estimating the surface density of adsorbed molecules. Independent detection of the resonance shifts for two polarization modes—transverse electric (TE) and transverse magnetic (TM)—is expected to allow us to estimate the orientation of adsorbed anisotropic molecules (21).

Each WGM is specified by l, m, ν, and polarization (22). l represents the number of waves in a circular orbit, m ($= -l, -l + 1, \ldots, l$) is the azimuthal index, and ν is equal to the number of peaks in the radial function of the electric field intensity, thus specifying the radial mode. The polarization is either TE or TM. The wavelength at resonance is determined by l, ν, and polarization. In a perfect spherical resonator, modes of different m are degenerate. The shift of resonance wavelength in response to the environmental changes depends also on l, ν, and polarization (23). It was recently demonstrated that the observed shifts of TE modes due to RI changes in the surroundings were in agreement with the shifts calculated using the indices evaluated for the microsphere used (24).

More than a decade ago, Folan distinguished TE and TM shifts of WGM in a small polystyrene sphere levitated electrodynamically in air (25). Folan examined the change in the scattering spectrum as water condensed onto the polymer sphere for the two polarizations, but the difference between the two shifts was insignificant within experimental error.

In this report, we use side coupling of a core-exposed single-mode fiber to induce both TE and TM polarizations in a silica microsphere and measure the wavelength shifts when proteins are added to the surrounding fluid to adsorb onto the sphere surface. We find that the shifts are different for TE and TM and the ratio of the two shifts provides information on the state of adsorbed protein. We confirmed the polarization-sensitive

Submitted December 15, 2006, and accepted for publication February 15, 2007.

Address reprint requests to Iwao Teraoka, E-mail: teraoka@poly.edu.
Mayumi Noto's present address is Nantero Inc., Woburn, MA 01801.

0006-3495/07/06/4466/07 $2.00
doi: 10.1529/biophysj.106.103200

shifts by adding NaCl to the surroundings to cause a uniform increase of RI. The latter situation simulates adsorption of large objects such as mitochondria (17).

Recently developed dual polarization interferometry (DPI) (26–29) can provide information on the state of surface-bound proteins. DPI uses two polarizations of light transmitted through a pair of planar waveguides to find the RI and thickness of the adsorption layer, which in turn provide information on the protein conformation. To achieve a high sensitivity comparable to that of the surface plasmon resonance (SPR) instrument, DPI uses a large sensor area, ~150 mm^2. Our WGM sensor has a much smaller sensor area, typically <0.005 mm^2, yet easily surpasses the sensitivity of DPI and SPR in terms of adsorbed mass per unit area while retaining the capability to find the state of the adsorbate. More importantly, the WGM sensor allows easy interpretation of the resonance shift in terms of molecular parameters (21), without the need to assume an adsorption layer of uniform RI and thickness (26). Neutron reflectivity (7) is another method that macroscopically characterizes the adsorbed molecules as a whole, but its sensitivity and usefulness are limited.

Theoretical background

A plain microsphere of radius a and uniform relative permittivity $\varepsilon_{r1} = n_1^2$ is placed in a uniform medium of $\varepsilon_{r2} = n_2^2$ ($n_1 > n_2$). When the wavelength, λ, of WGM is much shorter than a, the electric field, $\mathbf{E}(\mathbf{r})$, of the WGM is mostly confined to the interior of the microsphere. However, the evanescent field extends into the surroundings to the depth of $\sim(\lambda/2\pi)(n_1^2 - n_2^2)^{-1/2}$, which polarizes the molecules in the immediate neighborhood of the microsphere surface. The resonance wavelength of WGM shifts from λ_0 to $\lambda_0 + \Delta\lambda$, when small molecules (much smaller than λ/n_2) adsorb onto the sphere surface to displace a part of the surrounding medium. The adsorbed molecules are polarized by $\mathbf{E}(|\mathbf{r}| = a_+)$, where a_+ indicates the exterior side of the sphere surface.

The fractional shift $\Delta\lambda/\lambda_0$ is equal to the ratio of the polarization energy in the adsorbed molecules to the total mode energy (12,15,21). In general, the TE and TM modes exhibit different shifts, as the TE mode has only a tangential component, $E_t(a)$ as $\mathbf{E}(a_+)$, whereas the TM mode has also a normal component, $E_n(a_+)$. For uniform adsorption of N_p molecules of excess polarizability, α, at a low surface density, the fractional shift of either mode is given as (21)

$$\frac{\Delta\lambda}{\lambda_0} = \frac{N_p\langle\alpha_{tt}E_t^2(a) + \alpha_{nn}E_n^2(a_+)\rangle}{2\varepsilon_0\int\varepsilon_r\,\mathbf{E}^*(\mathbf{r})\cdot\mathbf{E}(\mathbf{r})d\mathbf{r}}, \quad (1)$$

where α_{tt} and α_{nn} are the polarizability tensor components in directions of E_t and E_n, respectively, $\langle\ldots\rangle$ indicates the average on the sphere surface (for E_t and E_n) or the average with respect to the configuration of adsorbed molecules (for α_{tt} and α_{nn}), ε_0 is the vacuum permittivity, and the volume integral in the denominator covers the entire space (relative permittivity ε_r is ε_{r1} in the sphere; ε_{r2} elsewhere).

We showed earlier that the denominator in Eq. 1 is equal to $4\pi a^3\varepsilon_0(\varepsilon_{r1} - \varepsilon_{r2})\langle[E_t(a)]^2\rangle$ for the TE mode (21,23). Then, the fractional shift of the TE mode is given as

$$\Delta\lambda_{TE}/\lambda_0 = N_p(\langle\alpha_{tt}\rangle/\varepsilon_0)[4\pi a^3(\varepsilon_{r1} - \varepsilon_{r2})]^{-1}. \quad (2)$$

The shift is identical for all radial modes ($\nu = 1, 2, \ldots$). Since $N_p \propto a^2$ for a given surface density of adsorbates, $\Delta\lambda/\lambda_0 \propto a^{-1}$. There is a weak dependence of $\Delta\lambda_{TE}/\lambda_0$ on λ_0 through wavelength dispersions of α_{tt}, ε_{r1}, and ε_{r2}. For the TM mode, the denominator in Eq. 1 is calculated as $4\pi a^3\varepsilon_0(\varepsilon_{r1} - \varepsilon_{r2})(\langle[E_t(a)]^2\rangle + (\varepsilon_{r2}/\varepsilon_{r1})\langle[E_n(a_+)]^2\rangle)$ (21,23). The expression for the TM shift, $\Delta\lambda_{TM}$, is then obtained. The ratio $\Delta\lambda_{TM}/\Delta\lambda_{TE}$ is

$$\Delta\lambda_{TM}/\Delta\lambda_{TE} = (A_+ + \langle\alpha_{nn}\rangle/\langle\alpha_{tt}\rangle)/(A_+ + \varepsilon_{r2}/\varepsilon_{r1}) \quad (3)$$

for each pair of WGM having the same l and ν. Here, $A_+ \equiv \langle[E_t(a)]^2\rangle/\langle[E_n(a_+)]^2\rangle$ is the intensity anisotropy ratio of the evanescent field of the TM mode (right on the sphere surface). When $l \gg 1$, the following approximation is useful (21):

$$A_+ \cong 1 - (n_2k_0a/l)^2, \quad (4)$$

which may be further approximated as $A_+ \cong 1 - \varepsilon_{r2}/\varepsilon_{r1}$. The second approximation is not good except for the first-order radial modes ($\nu = 1$). The shift ratio given by Eq. 3 is insensitive to the dimension of the adsorbed molecule, as long as it is sufficiently smaller than λ_0/n_2.

We now evaluate Eq. 3 for a molecule of volume V_p and uniform, isotropic relative permittivity $\varepsilon_{rp} = n_p^2$. We consider five geometries of the molecule—a sphere, a rod (cylinder) standing vertically on the surface, a rod lying on the surface, a disk standing on the surface (edge-on), and a disk lying on the surface (face-on), as illustrated in Fig. 1. For now, we assume a low surface density of adsorbed molecules. The effect of interference from the dipoles induced at nearby adsorbed molecules will be discussed toward the end of this section.

For each of the five geometries, α_{nn} is definite: $\langle\alpha_{nn}\rangle = \alpha_{nn}$. For a sphere, a standing rod and a lying disk, α_{tt}, is also definite. For a lying rod and a standing disk, the orientation of the molecule on the surface relative to E_t varies from

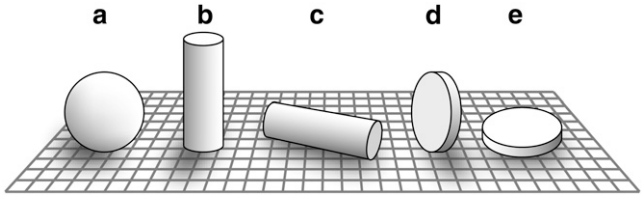

FIGURE 1 Five geometries of particles on a surface: (*a*) sphere, (*b*) standing rod, (*c*) lying rod, (*d*) standing disk (edge-on adsorption), and (*e*) lying disk (face-on adsorption).

molecule to molecule. If we assume random orientation of molecules in the directions tangential to the surface, $\langle\alpha_{tt}\rangle$ is the isotropic mean of the orthogonal tensor components in the directions parallel to the surface.

Table 1 lists $\langle\alpha_{tt}\rangle/(\varepsilon_0 V_p)$ and $\langle\alpha_{nn}\rangle/(\varepsilon_0 V_p)$ for the five geometries. These expressions were obtained from the boundary conditions for the electric field across the surface of the adsorbate. The expressions for the sphere and the two orientations of the rod were obtained earlier (21). Our early works also showed that the image dipole induced within the sphere does not affect the polarization of the adsorbed particle (21,30). For rods lying on the surface, $\langle\alpha_{tt}\rangle/(\varepsilon_0 V_p)$ is the isotropic mean of $2\varepsilon_{r2}(\varepsilon_{rp} + \varepsilon_{r2})^{-1}(\varepsilon_{rp} - \varepsilon_{f2})$ and $\varepsilon_{rp} - \varepsilon_{r2}$, which gives the listed expression. For edge-on adsorbed disks, $\langle\alpha_{tt}\rangle/(\varepsilon_0 V_p)$ is the isotropic mean of $(\varepsilon_{r2}/\varepsilon_{rp})(\varepsilon_{rp} - \varepsilon_{r2})$ and $\varepsilon_{rp} - \varepsilon_{r2}$. A thin uniform layer has the same α_{tt} and α_{nn} as those for isolated disks lying on the surface. The two geometries are listed in the last row of the table.

Table 1 also summarizes results for the shift ratio due to the shape anisotropy and lists its values for $\varepsilon_{r1} = 1.452^2$ (silica), $\varepsilon_{r2} = 1.32^2$ (water), $a = 171\ \mu m, \lambda_0 = 1.312\ \mu m, l = 1170$, and $\varepsilon_{rp} = 1.55^2$, where Eq. 4 was used for A_+. Here, the RI of protein at 1.32 μm was estimated as 1.55 from the value of 1.57 at 589 nm (31). More accurate calculation of the shift ratio employing the numerical method described earlier (21) gives the same values. The shift ratio for the sphere represents the ratio of the field intensities of the two modes on the surface and is nearly equal to $2 - \varepsilon_{r2}/\varepsilon_{r1}$. For the other geometries, the ratio is $2 - \varepsilon_{r2}/\varepsilon_{r1} = 1.18$ at $n_p = n_2$ and deviates from that value with an increasing n_p. The shift ratio >1.18 indicates $\alpha_{nn} > \alpha_{tt}$, which is likely due to molecules of an anisotropic shape standing on the surface. The ratio smaller than 1.18 indicates a geometry of the adsorbate extending parallel to the surface. The capability of the WGM sensors to provide information on the molecular orientation, independent of the size of the molecule, will be useful in studies on protein adsorption in different solutions and surface environments as well as conformational changes.

The above discussion applies to low surface coverages. With an increasing surface density, dipolar fields by nearby particles decrease $\langle[E_n(a_+)]^2\rangle$ but increase $\langle[E_t(a)]^2\rangle$ (21). Earlier (30), we used dipolar approximation to consider the effect for spherical molecules sequentially and randomly adsorbed onto the surface. Since we do not have a formula for geometries other than spheres, we adopt a formula for the spheres. Calculations for spheres of $n_p = 1.55$ show that the effect increases $E_t(a)$ by 0.9% and decreases $E_n(a_+)$ by 1.8% at 15% coverage of the projection of the spheres onto the surface. As a result, the TE shift is 0.9% greater than the estimate given by Eq. 2, and the TM shift is 1.3% less. The increase in A_+ with an increasing surface density causes the ratio to drop to 1.07 at the highest surface coverage in random sequential adsorption (32–34). Concomitantly, the criterion of the shift ratio for the anisotopic polarizability moves to a smaller value.

MATERIALS AND METHODS

Materials

Bovine serum albumin (BSA; A2153) was purchased from Sigma (St. Louis, MO). A 50 μmol/L solution of BSA in phosphate buffered saline (PBS) at pH 7.4 was prepared immediately before resonance shift measurements. Microspheres of radius around 200 μm were prepared by melting a tip of a single mode silica fiber (SMF-28; Corning, Corning, NY). Details of the microsphere preparation can be found elsewhere (12). The surface of microspheres used in BSA adsorption was modified with aminopropyltriethoxysilane. Microspheres used in NaCl experiments were washed in pyrranhia solution. The diameter of each microsphere was evaluated under an optical microscope to a reference of the optical fiber of cladding diameter 125 μm.

WGM resonance shift measurement system

The optical part in our measurement system is shown in Fig. 2. We used a pigtailed butterfly laser (distributed feedback laser; DFB) from NTT Electronics (NLK1B5E1AA; Saddle Brook, NJ) operating at $\sim$1.31 μm as a light source. The laser is linearly polarized with an extinction ratio $\sim$1000 as observed by a photodiode (PDA400; Thorlabs, Newton, NJ) at the end of the single-mode fiber. Exposing the core of the fiber by etching in hydrofluoric acid solution decreased the extinction ratio to $\sim$200. However, neither etching nor contact with the microsphere skewed the polarization. Rotation of the laser mount around the axis of the output fiber changed the polarization direction. The angle of rotation of the polarizer at the photodiode to maximize the intensity of transmitted light was measured as the laser mount was rotated in a step of 10° up to ±90° from the unstrained direction. The required polarizer rotation was nearly identical to the laser rotation. The standard deviation of the difference between the two angles of rotation was 4.8°. The extinction ratio barely changed during the rotation. Thus, we know what angles of the laser mount cause vertical and horizontal polarizations in the etched section of the fiber, which in turn will excite TE and TM modes, respectively, within the microsphere that touches the fiber at its horizontal equator.

TABLE 1 TM/TE shift ratio in adsorption of small molecules at low densities

			$\Delta\lambda_{TM}/\Delta\lambda_{TE}$	
Adsorbate	$\langle\alpha_{tt}\rangle/(\varepsilon_0 V_p)$	$\langle\alpha_{nn}\rangle/(\varepsilon_0 V_p)$	Formula	At $n_p = 1.55$
Spheres	$3\varepsilon_{r2}(\varepsilon_{rp} + 2\varepsilon_{r2})^{-1}(\varepsilon_{rp} - \varepsilon_{r2})$	$3\varepsilon_{r2}(\varepsilon_{rp} + 2\varepsilon_{r2})^{-1}(\varepsilon_{rp} - \varepsilon_{r2})$	$(A_+ + 1)/(A_+ + \varepsilon_{r2}/\varepsilon_{r1})$	1.18
Rods, standing	$2\varepsilon_{r2}(\varepsilon_{rp} + \varepsilon_{r2})^{-1}(\varepsilon_{rp} - \varepsilon_{r2})$	$\varepsilon_{rp} - \varepsilon_{r2}$	$[A_+ + (\varepsilon_{rp} + \varepsilon_{r2})/(2\varepsilon_{r2})]/(A_+ + \varepsilon_{r2}/\varepsilon_{r1})$	1.37
Rods, lying	$[\varepsilon_{r2}(\varepsilon_{rp} + \varepsilon_{r2})^{-1} + 1/2](\varepsilon_{rp} - \varepsilon_{r2})$	$2\varepsilon_{r2}(\varepsilon_{rp} + \varepsilon_{r2})^{-1}(\varepsilon_{rp} - \varepsilon_{r2})$	$[A_+ + 4\varepsilon_{r2}/(\varepsilon_{rp} + 3\varepsilon_{r2})]/(A_+ + \varepsilon_{r2}/\varepsilon_{r1})$	1.09
Disks, standing (edge-on)	$(1/2)(\varepsilon_{r2}/\varepsilon_{rp} + 1)(\varepsilon_{rp} - \varepsilon_{r2})$	$\varepsilon_{rp} - \varepsilon_{r2}$	$[A_+ + 2\varepsilon_{rp}/(\varepsilon_{rp} + \varepsilon_{r2})]/(A_+ + \varepsilon_{r2}/\varepsilon_{r1})$	1.34
Disks, lying (face-on); thin uniform layer	$\varepsilon_{rp} - \varepsilon_{r2}$	$(\varepsilon_{r2}/\varepsilon_{rp})(\varepsilon_{rp} - \varepsilon_{r2})$	$(A_+ + \varepsilon_{r2}/\varepsilon_{rp})/(A_+ + \varepsilon_{r2}/\varepsilon_{r1})$	0.90

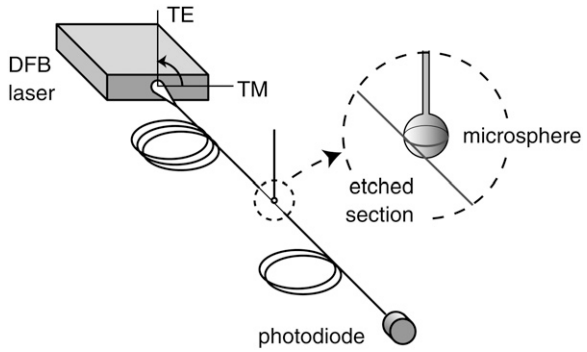

FIGURE 2 Optical part of microsphere WGM resonance shift measurement system that allows change of the polarization. A zoomed view of the fiber-microsphere coupling is also shown.

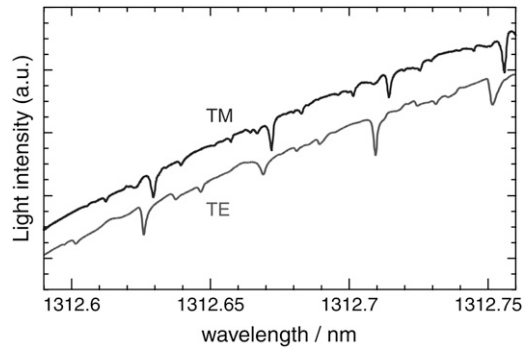

FIGURE 3 Light intensity through the fiber in the wavelength scan for TE and TM modes. The microsphere of 195-μm radius was immersed in water.

The other parts of the measurement system are similar to those described earlier (18). For this study, the laser wavelength, λ, was scanned at 10 Hz by changing the laser drive current, i, linearly with time. A sawtooth function generator was used for that purpose. The scan range was ~0.2 nm. The relationship between λ and i was evaluated using an interferometer (Agilent, Santa Clara, CA; HP3325A). In each scan, the laser intensity and wavelength increase almost linearly with time, and the two increases are nearly parallel to each other. When a microsphere is placed in contact with the core-exposed section of the fiber, destructive interference by the WGM causes dips in the light intensity at the photodetector. Each dip represents a WGM of a unique set of indices (l, m, ν, polarization).

RESULTS AND DISCUSSION

TE and TM spectra

In each experiment, the position of a microsphere relative to the fiber was adjusted to produce dips of reasonable depths in the wavelength scan of the light intensity through the fiber. Examples of the TE and TM spectra of the photodiode signal when the DFB laser was scanned by a current sweep, displayed in Fig. 3, are similar. Each spectrum has a period of ~0.042 nm, ascribed to splitting of the degenerate azimuthal modes (m) by a spheroidal shape of the microsphere; Lai et al. predicted polarization-independent splitting by distortion of the meridional cross section of the microspheroid (35). There is a major dip and several minor dips in each period. The major dips are for $\nu = 1$. Our scan range of ~0.2 nm sees just a part of a cluster of the dips having the same l but different values of m. The minor dips are ascribed to higher order radial modes ($\nu = 2, 3$; l may be different) and a tail portion of adjacent clusters with $\nu = 1$ (l is different by 1).

Adsorption of BSA

One of the microspheres (radius $a = 167$–203 μm) whose surface was modified with aminopropylsilane was immersed in a 980 μL solution of PBS at pH 7.4 that was constantly stirred and held at 25°C. For each adsorption study, a fresh microsphere was used. Resonance dips in the fiber transmission spectrum were traced as a 20 μL solution containing BSA (pI = 4.8) was added. The final concentration, 1 μmol/L, is sufficiently low to make the resonance shift due to the surroundings' RI change negligible compared with the shift due to adsorption but sufficiently high to cause the highest possible surface coverage for this pH and surface (18). We expect that the surface coverage is similar for all the microspheres. Fig. 4 shows typical changes of the TE and TM spectra. A part of the scan range is zoomed for clarity. The pair of experiments in Fig. 4 was selected so that the microsphere used for TM is slightly larger than the one used for TE. The intensity spectrum undergoes a red shift without changing the overall pattern. In either TE or TM mode, deep and shallow dips shift nearly equally. The TM shifts are greater than the TE shifts, although the sphere radius, a, is greater for TM; the shift is reciprocally proportional to a.

We did two measurements for TE and three for TM using spheres of different radii. To eliminate the radius dependence of the fractional shift, we compare the reduced fractional shift,

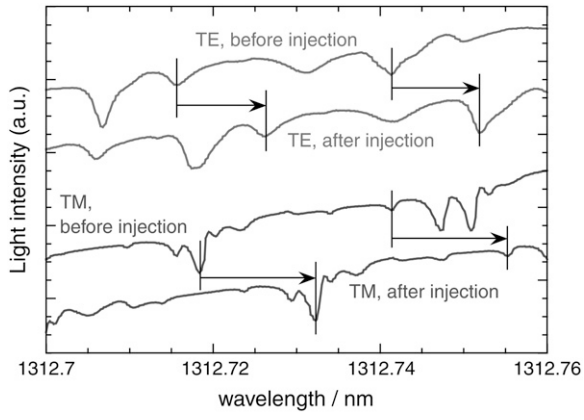

FIGURE 4 Light intensity spectrum before and after injection of BSA. The radii of the microspheres used for TE and TM modes are 167 μm and 186 μm, respectively. The arrows indicate the shifts for some dips.

$k_0a\Delta\lambda/\lambda_0$, where $k_0 = 2\pi/\lambda_0$ (k_0a is called a size parameter). From Eq. 2, we find that $k_0a\Delta\lambda/\lambda_0$ is proportional to the product of the number density of BSA on the surface and the polarizability. A similar relationship exists for the TM modes. In our TE mode experiments, $10^3k_0a\Delta\lambda/\lambda_0$ is 7.7 ± 0.1 (mean ± SD), regardless of whether the dip is deep or shallow. For the TM modes, the reduced shift is 10.3 ± 0.2. The shift's independence of the radial mode agrees with the theoretical prediction for adsorption of small particles (21). The ratio of the TM shift to the TE shift is 1.34, which is close to the ratios for standing rods and standing disks in Table 1. It is known that the BSA molecule is heart-shaped at pH = 7.4 (36). The result of our TE-TM shift study indicates adsorption of the heart-shaped molecule by one of its tips. At pH = 7.4, the protein surface has a high density of $-N^+H_3$ and COO^- (4), and the microsphere surface is dense with $-N^+H_3$. It is not surprising that the protein anchors to the aminopropyl surface by facing one of the sections covered predominantly with COO^- to the sphere surface. A study of protease digestion of BSA adsorbed on an unmodified silica surface at the same pH indicates a similar geometry (4), although sections predominantly covered with $-N^+H_3$ would face to $-SiO^-$ on the silica surface in the latter experiment.

The volume of a BSA molecule, V_p, is estimated from the molecular mass (1.10×10^{-19} g) and the specific volume of BSA, 0.734 g/cm^3 (37), as 81.0 nm^3. To estimate the surface coverage of BSA from our experimental data, we use below a picture of a standing disk with radius R and height H. First, we note that the above V_p can be equated to a disk of $R = 4.1$ nm, $H = 1.5$ nm, where the aspect ratio is close to the one proposed (38) in a phosphorescence study as consistent with x-ray crystallographic data (36). Then, from Table 1, we obtain $\alpha_{tt}/\varepsilon_0$ as 46.1 nm^3, where $\varepsilon_{r2} = 1.32^2$ and $\varepsilon_{rp} = 1.55^2$ were used. The surface density of the BSA molecules can be estimated using the formula

$$\frac{N_p}{4\pi a^2} = k_0 a \frac{\Delta\lambda_{TE}}{\lambda_0} \times \frac{\varepsilon_{r1} - \varepsilon_{r2}}{k_0\alpha/\varepsilon_0}. \quad (5)$$

Since $k_0 = 2\pi/\lambda_0 = 4.796\ \mu m^{-1}$, $\varepsilon_{r1} = 1.452^2$, and $k_0a(\Delta\lambda/\lambda_0)_{TE} = 7.7 \times 10^{-3}$ in our measurement, $N_p/(4\pi a^2)$ is estimated as $1.3 \times 10^4\ \mu m^{-3}$. Therefore, the area fraction Φ of the projection of the rectangular cross section $2RH$ onto the surface is estimated as $\Phi = [N_p/(4\pi a^2)]2RH = 0.15$. The latter value is <1/3 of the highest possible value of Φ by spheres, 0.55 (30,32–34).

We could assume another geometry for the BSA molecule, for instance, a standing rod. The molecular dimension of the rod that gives $V_p = 81.0$ nm^3 is $R = 1.9$ nm and $H = 7.1$ nm, for example. Then, $\alpha_{tt}/\varepsilon_0 = 44.9$ nm^3, virtually identical to the one we obtained for the disk model.

As discussed earlier, $\Phi = 0.15$ is too low for the dipoles induced in nearby particles to affect the estimate of Φ or the TM/TE shift ratio. Therefore, we do not need to change our discussion for the surface density and orientation of the adsorbed BSA molecules.

Refractive index change of the surroundings

We tested our polarization-sensitive WGM sensor for a uniform change of relative permittivity, Δn_2^2, in the surroundings. The change mimics adsorption of particles with a linear dimension greater than the penetration depth of the evanescent field. The shift will be greater for the mode with a greater ν, since its evanescent field penetrates deeper into the surroundings. Numerical calculation of the resonance conditions (23) gives the reduced response, $k_0a\Delta\lambda/(\lambda_0\Delta n_2^2)$, of the TE mode in a microsphere with $a = 174\ \mu$m at $\lambda_0 = 1.312\ \mu$m as 2.507 and 2.755 for $\nu = 1$ and 2, respectively. The reduced response of the TM mode will be 2.950 and 3.252 for $\nu = 1$ and 2, respectively. The reduced response is insensitive to a: At $a = 196\ \mu$m, the response for $\nu = 1$ is ~0.9% less than it is at $a = 174\ \mu$m.

In adding NaCl to the surroundings three times, the shifts exhibited a complicated pattern, as each radial mode had a different shift. Two parts of Fig. 5 show $10^3k_0a\Delta\lambda/\lambda_0$ for TE and TM modes as a function of NaCl concentration c in PBS buffer surrounding a plain silica microsphere ($a = 174$–$196\ \mu$m). The data were compiled from the shifts of different dips in a few measurements. Attention was paid not to include broad dips that apparently consisted of two or more dips at any stage of NaCl addition; the shape of these dips changed as more NaCl was introduced.

In Fig. 5, the shift for each dip in successive NaCl addition follows a straight line through the origin. The slope of the line is slightly different for each dip. The variations are ascribed to uncertainties in c and a and fluctuations in the resonance position. For the TE mode (Fig. 5 *a*), most of the data run along the lower solid line, ascribed to the $\nu = 1$ modes. The line gives $10^3k_0a\Delta\lambda/(\lambda_0\Delta c) = 0.990$ L/g. With $k_0a\Delta\lambda/\lambda_0 = 2.507 \times 2n_2\Delta n_2$, we obtain $dn/dc = 0.150$ mL/g,

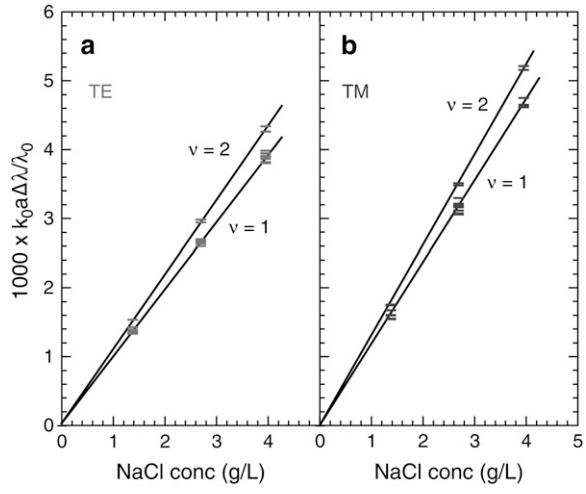

FIGURE 5 Fractional wavelength shift times the size parameter for (*a*) TE and (*b*) TM modes when a 20 μL, 0.0163 g/mL solution of NaCl is incrementally added to a buffer surrounding a silica microsphere. The lines are the best fit for two groups of data.

slightly less than 0.171 mL/g, the value reported for $\lambda = 589$ nm at 25°C (39). We believe that the difference is mostly due to RI dispersion. Likewise, most of the data run along the lower solid line in the plot for TM modes (Fig. 5 *b*). The ratio of the TM slope to the TE slope is 1.19, close to the theoretical value of 1.18.

In both of TE and TM plots, two sets of data are away from those for $\nu = 1$. They are ascribed to the $\nu = 2$ modes. The ratio of $k_0 a\Delta\lambda/(\lambda_0\Delta c)$ for these sets to that for $\nu = 1$ is 1.11 in TE and TM. The ratio compares favorably with the theoretical values.

CONCLUSIONS

We have demonstrated a simple method to excite TE and TM modes separately in a microsphere and observe the shifts of resonance lines when protein molecules adsorb at high densities. Studies of protein adsorption on different surface chemistries in different pH at different surface coverages will help us understand the state of protein on the surface. In particular, studies at low coverages will be important, as the TM/TE shift ratio allows us to estimate the polarizability anisotropy ratio of isolated molecules. The studies will be facilitated by simultaneous observation of the TE and TM shifts for a common microsphere which can be accomplished by feeding the light linearly polarized at ~45° from the TE direction, splitting the light by the polarizations right before the photodetector, and measuring the fiber transmission spectra using two photodiodes. The high sensitivity of the WGM sensor will allow such measurements at extremely low coverages of small molecules.

We thank L. Folan for helpful discussion.

This work was supported by the National Science Foundation through BES0522668.

REFERENCES

1. Nakanishi, K., T. Sakiyama, and K. Imamura. 2001. On the adsorption of proteins on solid surfaces, a common but very complicated phenomenon. *J. Biosci. Bioeng.* 91:233–244.
2. Gray, J. J. 2004. The interaction of proteins with solid surfaces. *Cur. Op. Str. Bio.* 14:110–115.
3. Robers, M., I. J. A. M. Rensink, C. E. Hack, L. A. Aarden, C. P. M. Reutelingsperger, J. F. C. Glatz, and W. Th. Hermens. 1999. A new principle for rapid immunoassay of proteins based on in situ precipitate-enhanced ellipsometry. *Biophys. J.* 76:2769–2776.
4. Larsericsdotter, H., S. Oscarsson, and J. Buijs. 2005. Structure, stability, and orientation of BSA adsorbed to silica. *J. Coll. Interf. Sci.* 289:26–35.
5. Malmsten, M. 1995. Ellipsometry studies of fibronectin adsorption. *Coll. Surf. B.* 3:371–381.
6. Sukhishvili, S. A., and S. Granick. 1999. Adsorption of human serum albumin: dependence on molecular architecture of the oppositely charged surface. *J. Chem. Phys.* 110:10153–10161.
7. Lu, J. R. 1999. Neutron reflection study of globular protein adsorption at planar interfaces. *Annu. Rep. Progr. Chem. Sec. C.* 95:3–45.
8. Giacomelli, C. E., M. G. E. G. Bremer, and W. Norde. 1999. ATR-FTIR study of IgG adsorbed on different silica surfaces. *J. Coll. Interf. Sci.* 220:13–23.
9. Giacomelli, C. E., and W. Norde. 2001. The adsorption-desorption cycle. Reversibility of the BSA-silica system. *J. Coll. Interf. Sci.* 233: 234–240.
10. Noinville, S., M. Revault, M.-H. Baron, A. Tiss, S. Yapoudjian, M. Ivanova, and R. Verger. 2002. Conformational changes and orientation of Humicola lanuginosa lipase on a solid hydrophobic surface: an in situ interface Fourier transform infrared-attenuated total reflection study. *Biophys. J.* 82:2709–2719.
11. Su, T. J., J. R. Lu, R. K. Thomas, Z. F. Cui, and J. Penfold. 1998. The conformational structure of bovine serum albumin layers adsorbed at the silica-water interface. *J. Phys. Chem. B.* 102:8100–8108.
12. Vollmer, F., D. Braun, A. Libchaber, M. Khoshsima, I. Teraoka, and S. Arnold. 2002. Protein detection by optical shift of a resonant microcavity. *Appl. Phys. Lett.* 80:4057–4059.
13. Armani, A. M., D. K. Armani, B. Min, K. J. Vahala, and S. M. Spillane. 2005. Ultra-high-Q microcavity operation in H_2O and D_2O. *Appl. Phys. Lett.* 87:151118.
14. Serpengüzel, A., S. Arnold, and G. Griffel. 1995. Excitation of resonances of microspheres on an optical fiber. *Opt. Lett.* 20:654–656.
15. Arnold, S., M. Khoshsima, I. Teraoka, S. Holler, and F. Vollmer. 2003. Shift of whispering-gallery modes in microspheres by protein adsorption. *Opt. Lett.* 28:272–274.
16. Vollmer, F., S. Arnold, D. Braun, I. Teraoka, and A. Libchaber. 2003. Multiplexed DNA detection by optical resonances in microspheres. *Biophys. J.* 85:1974–1979.
17. Noto, M., F. Vollmer, D. Keng, I. Teraoka, and S. Arnold. 2005. Nanolayer characterization through wavelength multiplexing of a microsphere resonator. *Opt. Lett.* 30:510–512.
18. Noto, M., M. Khoshsima, D. Keng, I. Teraoka, V. Kolchenko, and S. Arnold. 2005. Molecular weight dependence of a whispering gallery mode biosensor. *Appl. Phys. Lett.* 87:223901.
19. Teraoka, I., and S. Arnold. 2006. Enhancing sensitivity of a whispering gallery mode microsphere sensor by a high-refractive index surface layer. *J. Opt. Soc. Am. B.* 23:1434–1441.
20. Gaathon, O., J. Culic-Viskota, M. Mihnev, I. Teraoka, and S. Arnold. 2006. Enhancing sensitivity of a whispering gallery mode bio-sensor by sub-wavelength confinement. *Appl. Phys. Lett.* 89:223901.
21. Teraoka, I., and S. Arnold. 2006. Theory on resonance shifts in TE and TM whispering gallery modes by non-radial perturbations for sensing applications. *J. Opt. Soc. Am. B.* 23:1381–1389.
22. Johnson, B. R. 1993. Theory of morphology-dependent resonances: shape resonances and width formulas. *J. Opt. Soc. Am. A.* 10:343–352.
23. Teraoka, I., S. Arnold, and F. Vollmer. 2003. Perturbation approach to resonance shifts of whispering galley modes in a dielectric microsphere as a probe of a surrounding medium. *J. Opt. Soc. Am. B.* 20: 1937–1946.
24. Hanumegowda, N. M., C. J. Stica, B. C. Patel, I. White, and X. Fan. 2005. Refractometric sensors based on microsphere resonators. *Appl. Phys. Lett.* 87:201107.
25. Folan, L. M. 1992. Characterization of the accretion of material by microparticles using resonant ellipsometry. *Appl. Opt.* 31:2066–2071.
26. Swann, M. J., L. L. Peel, S. Carrington, and N. J. Freeman. 2004. Dual-polarization interferometry: an analytical technique to measure changes in protein structure in real time, to determine the stoichiometry of binding events, and to differentiate between specific and nonspecific interactions. *Anal. Biochem.* 329:190–198.
27. Freeman, N. J., L. L. Peel, M. J. Swann, G. H. Cross, A. Reeves, S. Brand, and J. R. Lu. 2004. Real time, high resolution studies of protein adsorption and structure at the solid-liquid interface using dual polarization interferometry. *J. Phys. Condens. Matter.* 16:S2493–S2496.
28. Berney, H., and K. Oliver. 2005. Dual polarization interferometry size and density characterisation of DNA immobilisation and hybridisation. *Biosens. Bioelectron.* 21:618–626.

29. Ricard-Blum, S., L. L. Peel, F. Ruggiero, and N. J. Freeman. 2006. Dual polarization interferometry characterization of carbohydrate-protein interactions. *Anal. Biochem.* 352:252–259.

30. Teraoka, I., and S. Arnold. 2007. Dielectric property of particles at interface in random sequential adsorption and its application to whispering gallery mode resonance-shift sensors. *J. Appl. Phys.* 101:023505.

31. Vörös, J. 2004. The density and refractive index of adsorbing protein layers. *Biophys. J.* 87:553–561.

32. Onoda, G. Y., and E. G. Liniger. 1986. Experimental determination of the random-parking limit in two dimensions. *Phys. Rev. A.* 33:715–716.

33. Wang, J. S. 1994. A fast algorithm for random sequential adsorption of discs. *Int. J. Mod. Phys. C.* 5:707–715.

34. Torquato, S. 1995. Mean nearest-neighbor distance in random packings of hard d-dimensional spheres. *Phys. Rev. Lett.* 74:2156–2159.

35. Lai, H. M., P. T. Leung, K. Young, P. W. Barber, and S. C. Hill. 1990. Time-independent perturbation for leaking electromagnetic modes in open systems with application to resonances in microdroplets. *Phys. Rev. A.* 41:5187–5198.

36. Carter, D. C., and J. X. Ho. 1994. Structure of serum albumin. *Adv. Protein Chem.* 45:153–196.

37. Brill, A. S., J. S. Olin, and B. M. Siegel. 1962. The specific volume of dry protein. *J. Cell Biol.* 13:249–251.

38. Ferrer, M. L., R. Duchowicz, B. Carrasco, J. García de la Torre, and A. U. Acuña. 2001. The conformation of serum albumin in solution: a combined phosphorescence depolarization-hydrodynamic modeling study. *Biophys. J.* 80:2422–2430.

39. Russo, P. Differential Index of Refraction, *dn*/*dc*. http://macro.lsu.edu/HowTo/.